









Mapping tropical forest functional variation at satellite remote sensing resolutions depends on key traits

Elsa M. Ordway ^{1,2✉}, Gregory P. Asner ³, David F. R. P. Burslem ⁴, Simon L. Lewis ^{5,6}, Reuben Nilus⁷, Roberta E. Martin ³, Michael J. O'Brien ⁸, Oliver L. Phillips ⁵, Lan Qie⁹, Nicholas R. Vaughn ³ & Paul R. Moorcroft¹

Although tropical forests differ substantially in form and function, they are often represented as a single biome in global change models, hindering understanding of how different tropical forests will respond to environmental change. The response of the tropical forest biome to environmental change is strongly influenced by forest type. Forest types differ based on functional traits and forest structure, which are readily derived from high resolution airborne remotely sensed data. Whether the spatial resolution of emerging satellite-derived hyperspectral data is sufficient to identify different tropical forest types is unclear. Here, we resample airborne remotely sensed forest data at spatial resolutions relevant to satellite remote sensing (30 m) across two sites in Malaysian Borneo. Using principal component and cluster analysis, we derive and map seven forest types. We find ecologically relevant variations in forest type that correspond to substantial differences in carbon stock, growth, and mortality rate. We find leaf mass per area and canopy phosphorus are critical traits for distinguishing forest type. Our findings highlight the importance of these parameters for accurately mapping tropical forest types using space borne observations.

¹Department of Organismic and Evolutionary Biology, Harvard University, 26 Oxford Street, Cambridge, MA 02138, USA. ²Department of Ecology and Evolutionary Biology, UCLA, 612 Charles E. Young Drive South, Los Angeles, CA 90095, USA. ³Center for Global Discovery and Conservation Science, Arizona State University, 60 Nowelo St, Hilo, HI 96720, USA. ⁴School of Biological Sciences, University of Aberdeen, Aberdeen AB24 3UU, UK. ⁵School of Geography, University of Leeds, Leeds LS2 9JT, UK. ⁶Department of Geography, University College London, London WC1E 6BT, UK. ⁷Sabah Forestry Department, Forest Research Centre, Sandakan, Sabah, Malaysia. ⁸Área de Biodiversidad y Conservación, Universidad Rey Juan Carlos, c/ Tulipán s/n., E-28933 Móstoles, Spain. ⁹School of Life and Environmental Sciences, University of Lincoln, Lincoln LN6 7DL, UK. ✉email: elsaordway@ucla.edu

Tropical forests are the most biologically diverse biome on Earth, encompassing an estimated 96% of all tree species¹. Although categorized as a single biome, tropical forests differ substantially within and across continents. Differences in ecosystem structure and function corresponding to variation in species composition directly influence ecosystem processes and will likely influence tropical forest responses to climate change. For example, field observations indicate that the carbon sink in tropical Africa has been stable for three decades (1983–2011), which is in stark contrast with a long-term decline in the Amazon². However, a study using Orbiting Carbon Observatory (OCO-2) satellite data revealed net carbon emissions across Africa, Asia, and the Americas following the 2015 El Niño event, albeit with unique drivers³. The ability to map and characterize distinct tropical forest types is thus critical for identifying where further research can examine mechanistic controls on differences in structure and function, and how different forest types within the tropical forest biome will respond to a changing planet. This is of particular importance as tropical forests are threatened by deforestation, degradation, and climate change, and are critical for carbon sequestration and many other important ecosystem services.

Networks of tropical forest inventory plots offer valuable ground-based insights into mechanisms and processes. However, remote sensing data can be used to scale these insights to entire landscapes and regions and highlight previously unexplored areas for further investigation of mechanism and process. Remote sensing can thus serve as a powerful tool to measure and map functionally distinct forest types across the tropics that may be inaccessible for ground-based investigation. The recent surge in ecologically orientated satellite remote sensing missions, including spaceborne LiDAR (i.e., light detection and ranging) and imaging spectroscopy (i.e., hyperspectral remote sensing), makes this a critical moment to evaluate tropical forest function mapping at spaceborne resolutions (e.g., ~20–30 m) and assess the relative importance of forest structure and canopy leaf traits for characterizing tropical forest function.

Forest types in the tropics differ in canopy structure and function, which vary with climate⁴, topography⁵, soil biogeochemistry^{6,7}, and natural and anthropogenic disturbance histories and regimes^{8,9}. Airborne imaging spectroscopy and LiDAR have enabled the measuring, mapping, and monitoring of tropical forest functional and structural diversity at large spatial scales, in ways that inform ecological understanding^{10,11}, support conservation efforts¹², and constrain terrestrial biosphere models¹³. In the tropics, airborne imaging spectroscopy has been used to map patterns of diversity across forests in Borneo¹¹ and the Amazon^{10,14}. Airborne imaging spectroscopy has also been used to characterize leaf traits across the sunlit portions of tropical forest canopies that are detectable by a satellite or airborne sensor (which we refer to here as canopy traits) and identify relationships between these traits and underlying environmental drivers. For example, Asner and coauthors¹² identified relationships between imaging spectroscopy-derived canopy traits and variation in geology, topography, hydrology, and climate across the Peruvian Amazon, sorting the region into 36 distinct forest types. In Malaysia, airborne imaging spectroscopy and LiDAR data showed a strong influence of fine-scale topography on forest structure, composition and diversity⁵, and the role of interacting geomorphology and topography on canopy foliar traits across larger elevation gradients¹⁵.

Expanded research opportunities will be made possible by the newly available ecologically oriented hyperspectral and LiDAR satellite missions, including the operational PRISMA¹⁶ and DESIS¹⁷ spectrometers, NASA's Global Ecosystem Dynamics Investigation spaceborne LiDAR¹⁸, and the planned NASA Surface Biology Geology (SBG)¹⁹, and European Space Agency Copernicus

Hyperspectral Imaging Mission for the Environment (CHIME)²⁰ spaceborne spectrometers. Satellite instruments overcome expensive and spatially restricted airborne campaign limitations by providing extensive coverage over tropical forest regions. However, the data from these sensors are or will be at spatial resolutions of ~20–30 m (400–900 m²), far coarser than the 1–5 m (1–25 m²) resolutions of airborne remote sensing data used in the studies described above. In addition, lack of knowledge of what traits to prioritize to enable distinguishing between different tropical forest types hinders satellite sensor and algorithm development. Here, we hypothesize that functionally distinct forest types can be mapped using a combination of canopy foliar traits and canopy structure information using moderate (30 m) spatial resolution, equivalent to the resolution available via forthcoming satellite sensors (H1). We evaluate what canopy traits or structural attributes are most critical for mapping distinct forest types. We hypothesize that mapped forest types, distinguishable at the 30 m spatial resolution, exhibit distinct ecosystem function (H2) related to carbon stocks (H2a), growth (H2b), and mortality (H2c).

In this study, we combine airborne imaging spectroscopy-derived canopy trait measurements with airborne LiDAR-derived measurements of canopy structure, resampled to resolutions corresponding to new satellite missions (30 m) to (1) identify, characterize, and map structurally and functionally distinct tropical forests across two landscapes in Malaysian Borneo; (2) determine the key canopy traits and canopy structural attributes that distinguish different forest types; and (3) compare mapped forest types with inventory plot data to explore differences in carbon stocks, growth, and mortality within each forest type. We used canopy trait maps developed by Martin et al.²¹ that used co-aligned LiDAR and imaging spectroscopy data collected by the Global Airborne Observatory from an aircraft in April 2016²², and structural metrics that we calculated directly from the airborne LiDAR data (Supplementary Figs. 1 and 2). Canopy traits and structural attributes were selected to capture two main forest type trait axes, which explain roughly half of the global trait variation. These axes include plant stature and resource acquisitiveness, which are linked to tree growth and mortality tradeoffs^{23,24}. The canopy traits and structural attributes that we evaluated included leaf economic spectrum traits indicative of resource acquisition—leaf mass per area (LMA), leaf nitrogen (N), and leaf phosphorus (P), as well as stature—maximum canopy height, and crown and canopy architecture. To more directly evaluate canopy photosynthetic capacity, we estimated the maximum rate of Rubisco carboxylase activity (V_{cmax}) from canopy N, canopy P, and the ratio of N:P using a statistical equation described in ref. ²⁵ This enabled exploration of an additional axis of variation related more directly to the impacts of nutrient co-limitation on growth across forest types. However, it is important to note that this is a statistical estimate, and not a process-based model. In addition, we evaluated leaf area index (LAI) and variation in the height above ground of peak LAI in the canopy, given that LAI is an important ecophysiological attribute that is widely used in terrestrial ecosystem and biosphere models to upscale estimates of leaf-level processes^{26,27}.

To map functionally distinct forest types across all pixels, testing hypothesis one, we conducted a principal component analysis (PCA) to reduce dimensionality of all ten canopy traits and structural attributes (hereafter canopy properties), and ran a *k*-means cluster analysis²⁸ on the first two principal components to categorize pixels into functionally distinct forest types. To first evaluate the influence of spatial resolution on forest type mapping, we conducted analyses on canopy traits and structural attributes at their original resolution (4 m) and 15 coarse-scale resampled resolutions from 8 to 200 m. We used three methods to determine the appropriate number of clusters (*k*): (1) the gap statistic (Gap_{*k*}),

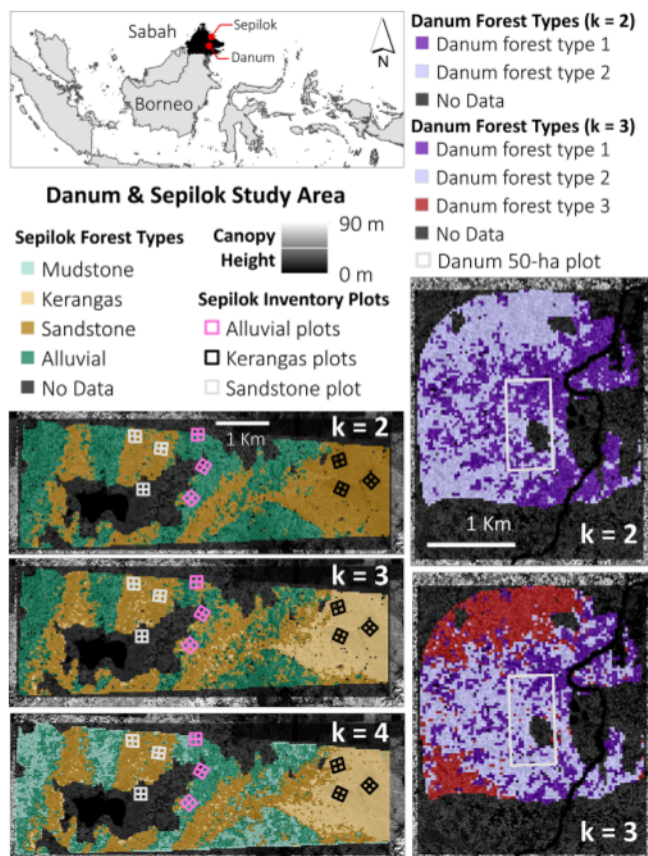


Fig. 1 Mapped forest types. Mapped forest type results from PCA and k -means clustering of 10 variables across forest ecosystems in Sepilok Forest Reserve for $k = 2, 3$, and 4 , and in Danum Valley Conservation Area around the 50 ha Smithsonian ForestGEO plot for $k = 2$ and 3 . Here, we omit the Danum $k = 1$ map, which would show a single color for the entire area, and instead highlight the difference between $k = 2$ and $k = 3$ cluster results. At Sepilok, the partitioning of the alluvial forest into alluvial and mudstone forest types is revealed with $k = 4$. The canopy height shading scale indicates the top-of-canopy height information from the airborne LiDAR. Black areas in the clustered forest type maps indicate No Data where pixels were omitted, or cloud, cloud shadow, and water masked.

which defines the number of clusters based on the first local and global maxima; (2) the elbow approach using the within group sum of squares (W_k), and (3) the between cluster sum of squares (BSS) divided by the total sum of squares (TSS), where a higher value of BSS/TSS indicates improved fit of the cluster analysis to the data. To test hypothesis two and evaluate whether clustered forest types exhibited distinct functional dynamics, we compared our forest functional composition maps to 4 ha inventory plot data established within three distinct forest types Sepilok and one large 50 ha inventory plot at Danum. We demonstrate that forest types can be successfully mapped using data at the 30 m spatial resolution corresponding to new hyperspectral satellite missions revealing biologically relevant heterogeneity in tropical forest structure and function. Two canopy traits—LMA and canopy foliar phosphorus—were found to be critical for accurately distinguishing between forest types, while structural characteristics were found to be of secondary importance.

Results

Our analysis identified between two and four distinct forest types in Sepilok, and a single forest type at Danum that could be further distinguished as three distinct forest types (Fig. 1). The influence

of spatial resolution on the degree of variance explained for the first 2–4 principal components and the k -means BSS/TSS saturated around 20–40 m resolution for both Sepilok and Danum (Supplementary Fig. 3). Here, we present results from analyses at the 30 m spatial resolution that corresponds to existing and forthcoming hyperspectral satellite missions.

At Sepilok, the Gap_k metric identified three clusters (BSS/TSS = 68.5%). However, the W_k elbow and BSS/TSS metrics suggest that Sepilok can also be characterized as two (BSS/TSS = 51.9%) or four (BSS/TSS = 76.7%) distinct forest types based on the magnitude of the decline in W_k , and gains in BSS/TSS before the values of both metrics level-off with increasing k (Supplementary Figs. 4 and 5). Cluster analysis results for differing values of k indicated nested forest types at Sepilok (Fig. 2a–c): the highest level ($k = 2$) distinguished an alluvial forest type from sandstone and *kerangas* forest type; $k = 3$ distinguished sandstone forests from *kerangas* forests; and $k = 4$ partitioned the alluvial forest into two forest types, revealing a mudstone forest type as distinct. At Danum, we identified a single cluster using the Gap_k metric (BSS/TSS = 0.0%); however, the W_k elbow BSS/TSS methods both indicate that Danum can be characterized as three distinct forest types (BSS/TSS = 61.3%; Figs. 1 and 2; Supplementary Figs. 4 and 5). Two of these forest types (Danum 1 and 2) were found within the 50 ha ForestGEO inventory plot when $k = 2$ and $k = 3$ (Fig. 1). The 50 ha inventory plot appears to be dominated by one forest type (Danum 2), although the northeast corner was identified as distinct (Danum 1) when $k = 2$ and $k = 3$ (Fig. 1; Supplementary Fig. 8).

Distinguishing characteristics of forest types. The first principal component (PC1) corresponded to variation in remotely sensed LMA in grams of dry mass per square meter (LMA, g DM m^{-2}), percent canopy leaf nitrogen (N, %), and percent canopy leaf phosphorus (P, %). The second principal component (PC2) reflected variation in remotely sensed canopy stature—maximum canopy height in meters (Max H, m) and the percent of canopy cover at 20 m height above ground (Cover₂₀, %), which corresponds to field measurements of basal area; a measure of canopy architecture indicating the vertical distribution of plant foliage (P) relative to the total canopy height (P:H ratio); and estimated photosynthetic capacity (V_{cmax} , $\mu\text{mol m}^{-2} \text{s}^{-1}$). These patterns were consistent at Danum and Sepilok (Fig. 2; Supplementary Fig. 6). Remotely sensed LAI (LAI, $\text{m}^2 \text{m}^{-2}$) explained little variation across the forest types, with weak loading values (PC3 at Sepilok, PC4 at Danum; Supplementary Fig. 6). Figure 3 shows variation in canopy properties across forest types, shown for the largest number of forest types identified at each landscape (i.e., $k = 3$ and $k = 4$; see Supplementary Figs. 7–9 for results from other values of k). The sandstone and *kerangas* forests had the lowest mean canopy leaf nutrient concentrations and estimated photosynthetic capacity (Fig. 3a – N, P, V_{cmax}). Despite having lower canopy height than other forest types, the sandstone and *kerangas* forests had the highest fraction of canopy cover above 20 m height, high P:H values, and the highest peak height of LAI ($H_{\text{peak LAI}}$, m) (Fig. 3a – Cover₂₀, P:H, $H_{\text{peak LAI}}$).

Strong gradients in LMA, canopy N, and canopy P were observed across all forest types. The highest canopy leaf nutrient concentrations and the lowest average LMA were observed in the three Danum forest types, and the Sepilok mudstone and alluvial forests (Fig. 3a – LMA). These patterns were consistent across different values of k (Supplementary Figs. 7 and 8). Average canopy N and P in the mudstone forest were equivalent to or higher than the alluvial forest, yet the mudstone forest had significantly lower estimated V_{cmax} . Significantly lower maximum canopy heights (max H) and greater foliage density near the

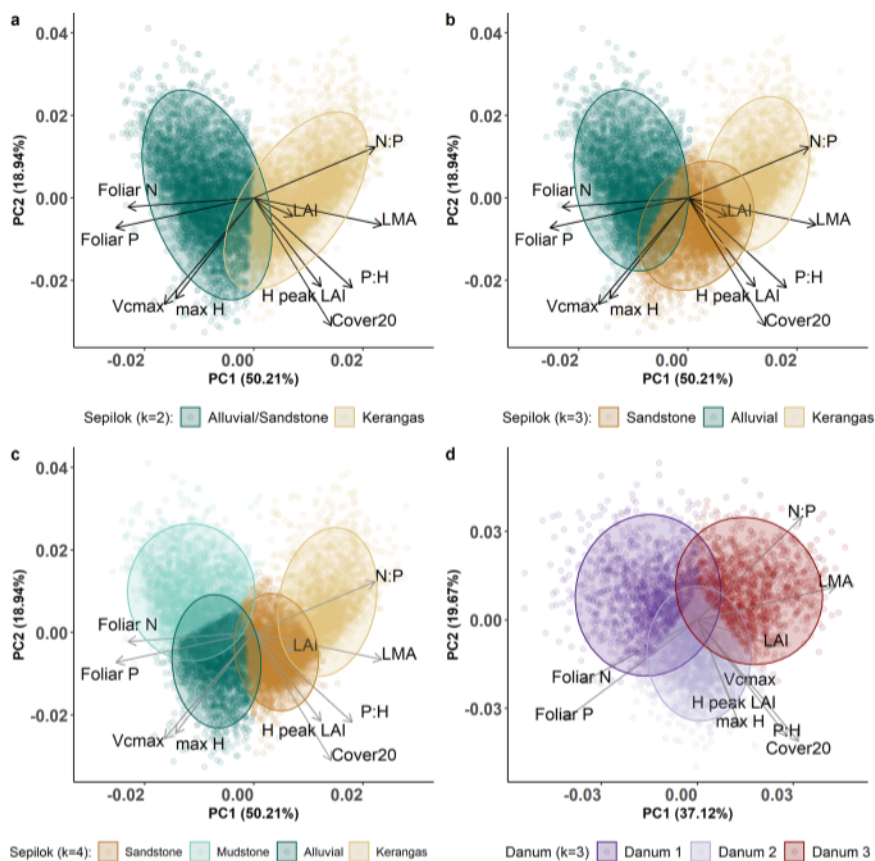


Fig. 2 Principal component analysis results. The first two loadings from the principal component analysis at Sepilok (**a–c**) and Danum (**d**). **a–c** illustrate the partitioning of pixels into $k = 2, 3$, and 4 clusters at Sepilok. **d** illustrates $k = 3$ clusters at Danum. Cover20: the percent of canopy cover at 20 m height above ground; H peak LAI: height of peak leaf area index, LAI: Leaf area index, LMA: Leaf mass per area, max H: maximum height, N: Nitrogen, N:P: Nitrogen to phosphorus ratio, P: Phosphorus, P:H: the vertical distribution of plant foliage (P) relative to the total canopy height (H).

ground (lower P:H) also distinguished the mudstone and Danum 1 forests from the alluvial and Danum 2–3 forests. The Danum 1 forest (when $k = 2$ or 3) was structurally similar to the mudstone forest; however, the two forest types differed in LMA, canopy N, canopy P (Fig. 3a).

While average canopy LAI was similar across forest types (Fig. 3a – LAI), ranging from 5.4 to 6.3, (coefficient of variation (CV) = 0.05), the average height of maximum LAI ($H_{\text{peak LAI}}$), canopy architecture (P:H), and canopy cover at 20 m (Cover_{20}) all exhibited much greater variation across forest types (CV = 0.48; 0.12; 0.25 respectively). Vertical LAI patterns further illustrated differences in structure across forest types despite similar total LAI (Fig. 3b, c, Supplementary Fig. 9), with strong clumping in the understory and the upper canopy at the alluvial and Danum forests. Vertical LAI profiles indicated less height heterogeneity in the sandstone and *kerangas* forests (Fig. 3b, c). Maximum canopy height, which varied significantly across clusters, was correlated with estimated V_{cmax} between the different forest types ($R^2 = 0.72$, $p = 0.017$) and at the pixel scale ($R^2 = 0.24$, $p < 0.0001$) (Supplementary Fig. 10). Given that V_{cmax} was estimated based on the linear relationship between canopy leaf N and P (i.e., not derived from leaf-level measurements as the other remotely sensed traits were—see Methods), it was thus surprising to find variation in the estimated canopy trait that was uncorrelated with either N or P.

Remotely sensed estimates of aboveground carbon density, an emergent property of ecosystem function, differed significantly across clustered forest types, with high values on average in sandstone forests and widely varying values in the alluvial and

Danum forest types (Fig. 4a). Aboveground carbon, in megagrams of carbon per hectare (MgC ha^{-1}), within the inventory plot boundaries generally corresponded to aboveground carbon distributions derived from the entire forest type (Fig. 4a). The one exception was the alluvial forest. When three forest types were distinguished at Sepilok ($k = 3$), the alluvial forest inventory plot had significantly higher aboveground carbon than the cluster-derived alluvial forest extent (Fig. 4a, $p < 0.001$). However, when the mudstone and alluvial forests were differentiated ($k = 4$), the inventory plot aboveground carbon distribution was comparable to aboveground carbon in the clustered alluvial forest extent. As a result, the mudstone forest encompassed significantly lower aboveground carbon on average. Annual relative growth and mortality rates calculated from forest inventory plot data differed significantly across forest types (Fig. 4b). Growth rates corresponded inversely to mean aboveground carbon at the sandstone (232 MgC ha^{-1}), alluvial (223 MgC ha^{-1}), and Danum 50 ha (194 MgC ha^{-1}) inventory plots (Fig. 4a, b). The *kerangas* forest did not follow this trend, exhibiting an intermediate plot-level growth rate despite lower average aboveground carbon (180 MgC ha^{-1}). Mortality rates were similar in the alluvial and Danum 50 ha plots, and significantly higher than the mortality rates in the sandstone or *kerangas* plots.

The relative importance of canopy traits and structural attributes. Cluster analyses conducted with only structural attributes, only canopy traits, or reduced combinations of canopy traits and structural attributes, indicated that leaf P, LMA, maximum canopy height and Cover_{20} are critical for capturing the observed forest types

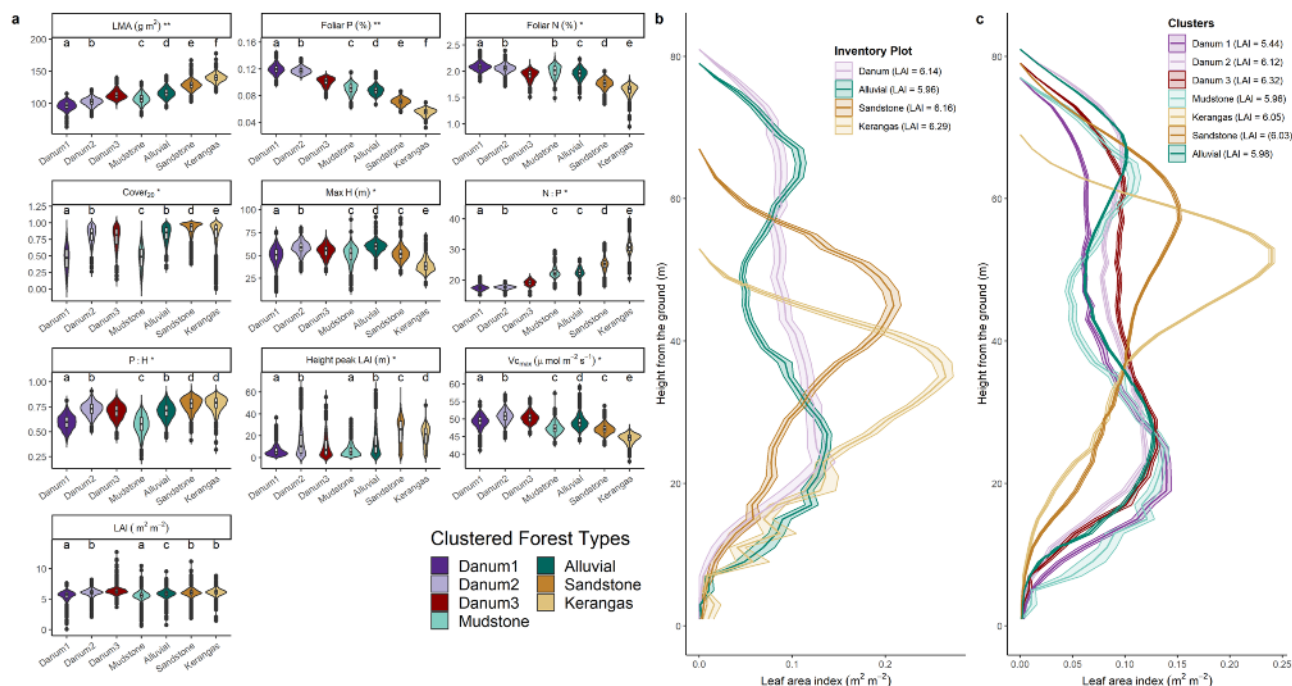


Fig. 3 Canopy trait and structural attribute distributions. Trait distributions by cluster for Sepilok $k = 4$ and Danum $k = 3$. Forest types are ordered based on their median leaf mass per area (LMA) to illustrate differences in traits for forest types that vary along the leaf economics spectrum. Identical letters represent clusters where there is no significant difference between forests based on one-way ANOVA tests ($p < 0.01$). ** = traits that varied significantly between all seven forest types. * = traits that varied significantly between at least five forest types (a). Vertical leaf area index (LAI) profiles for all pixels within each inventory plot (b) and forest types identified based on $k = 3$ clusters at Danum and $k = 4$ clusters at Sepilok (c). Shading around lines in b, c indicate 95% confidence interval.

(Fig. 5). Clustering with LMA, leaf P, Cover₂₀, and maximum height resulted in similar forest types to those identified when ten canopy properties were used (overall accuracies (OA) of 96.0% and 86.0% for $k = 2$ and $k = 4$ respectively) at Sepilok (Fig. 5a; Supplementary Fig. 11a), as well as higher BSS/TSS values at both Sepilok (Supplementary Fig. 12a) and Danum (Supplementary Fig. 12b). At Danum, LMA, leaf P, and Cover₂₀ alone yielded the strongest similarity to the cluster results with all ten variables (OA = 88.0%; Fig. 5b, Supplementary Fig. 11b). The highest overall accuracy for $k = 3$ at Sepilok was achieved with LMA, canopy leaf P, and N, equal to 85.9%, although the combination of maximum height, LMA and leaf P (OA = 84.8%), and just LMA and leaf P (OA = 84.7%) yielded similar results (Fig. 5a). We were unable to obtain distinct mapped forest types using structural attributes alone. The inclusion of leaf P improved output in all cases in terms of correspondence with plot locations and noise (speckling) reduction.

Discussion

We hypothesized that functionally distinct forest types can be mapped at moderate spatial resolutions, using a combination of canopy foliar traits and canopy structure information. Our analysis of LiDAR and imaging spectroscopy data at spatial resolutions ranging from 4 to 200 m (16 m²–40,000 m²), with an emphasis on the 30 m (900 m²) spaceborne hyperspectral spatial resolution, reveals that few remotely sensed canopy properties are needed to successfully identify ecologically distinct forest types at two diverse tropical forest sites in Malaysian Borneo. In testing our second hypothesis that mapped forest types exhibit distinct ecosystem function, we found that forest types identified using remotely sensed leaf P, LMA, Max H, and canopy cover at 20 m height (Cover₂₀) closely align with forest types defined from field-based floristic surveys^{29–33} and inventory plot-based measurements of growth and mortality rates (Fig. 4b). Our approach, however, enables mapping

of their entire spatial extent (Fig. 1) and reveals important structural and functional variation within areas characterized as a single forest type in previous studies (Fig. 3). Current and forthcoming satellite hyperspectral platforms, including PRISMA (30 m), CHIME (20–30 m), and SBG (30 m), have or will have comparable spectral resolution, higher temporal revisits, and much greater geographic coverage. The ability to conduct this type of analysis using remote sensing measurements at 30 m resolution suggests that our method can be applied to these emerging spaceborne imaging spectroscopy data to reveal important differences in structure and function across the world’s tropical forests.

Nested functional forest types revealed. To test our first hypothesis, rather than making an a priori decision about the number of k -means clusters (k), we explored the capacity of remotely sensed data to reveal ecologically relevant variation in forest types. Baldeck and Asner took a similar unsupervised approach to estimating beta diversity in South Africa³⁴. Because the choice of k directly influences analysis outcomes, careful selection of k is required. Different approaches for identifying the number of clusters, using the Gap_k and W_k elbow metrics³⁵, yielded varying optimal numbers of clusters for the Sepilok and Danum landscapes (Fig. 1, Supplementary Figs. 4 and 5). However, at both sites, a comparison of results based on different values of k revealed ecologically meaningful structural and functional differences and graduated transitions between forest types (Fig. 2, Supplementary Figs. 7 and 8), indicating that the exploration of traits that aggregate or separate forest types as k changes is a valuable exercise. Overlap between the remotely sensed forest type boundaries and inventory plots within distinct forest types indicate that the series of clustered forests align closely with forest types defined based on in situ data on species composition and ecosystem structure. In part, this type of analysis

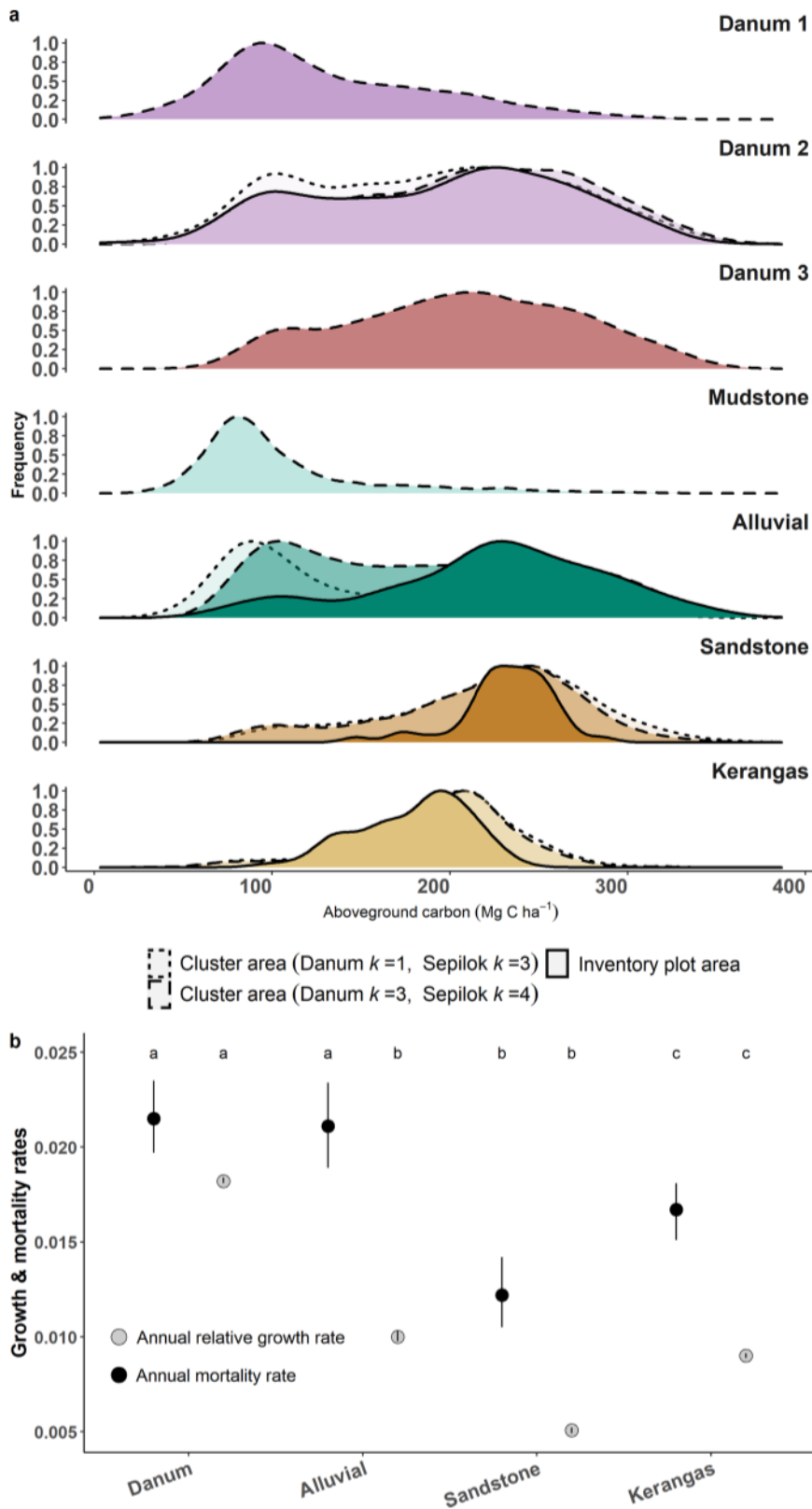


Fig. 4 Functional dynamics across forest types. **a** Aboveground carbon density for each field inventory plot (solid line) compared to aboveground carbon for the entire forest type based on cluster results where $k=1$ for Danum and $k=3$ for Sepilok (dotted line) and $k=3$ for Danum and $k=4$ for Sepilok (dashed line). **b** Annual relative growth (gray) and mortality (black) rates for each forest type calculated from forest inventory plot data. Growth and mortality rates could not be calculated for the Mudstone forest type due to the lack of an inventory plot with repeat census measurements. Identical letters represent inventory plots with no significant difference in terms of carbon, mortality rates, and growth rates respectively, based on one-way ANOVA tests ($p < 0.01$). Error bars in **b** indicate 95% confidence interval.

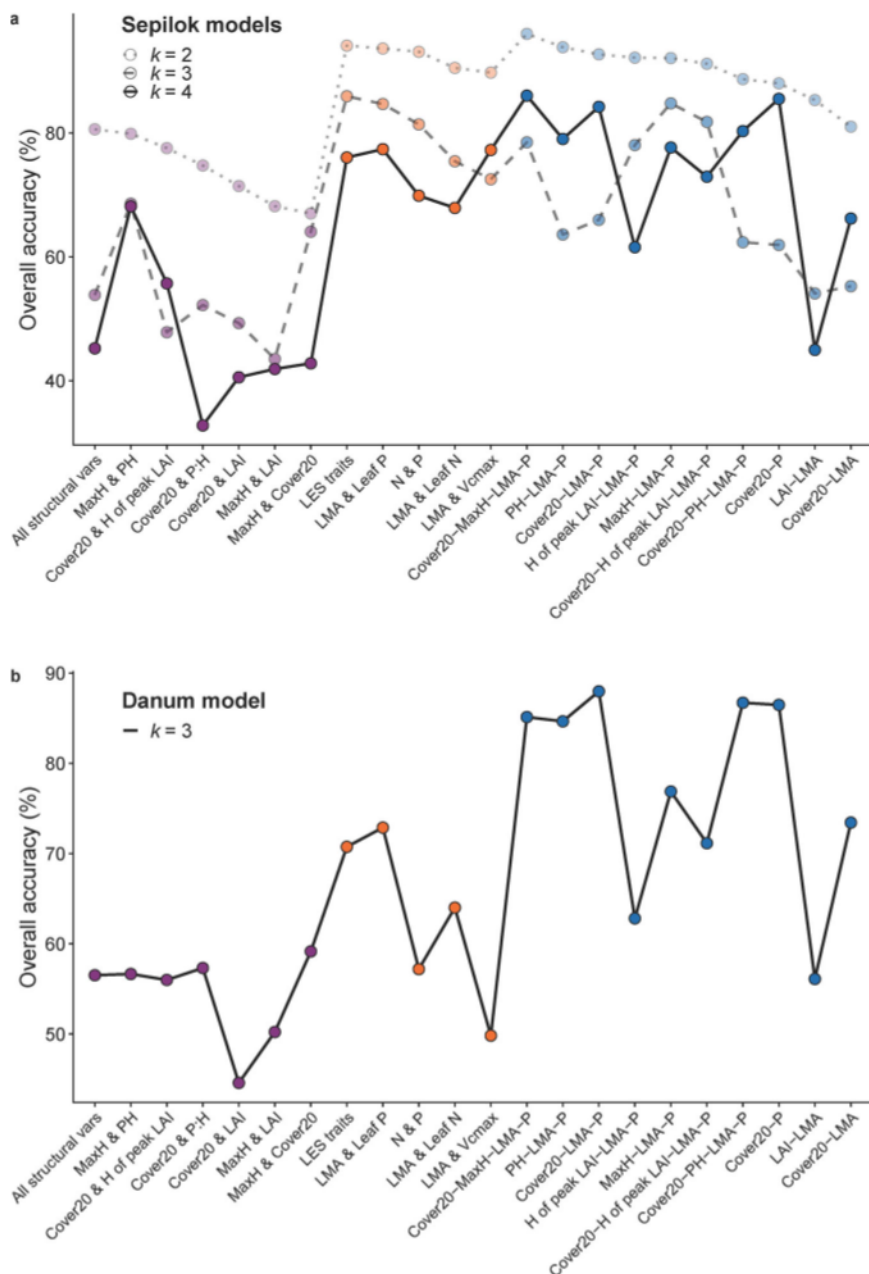


Fig. 5 Trait importance in forest type mapping. Change in overall accuracy for reduced *k*-means clustering models using forest structure variables (purple), canopy leaf trait variables (orange), and combinations of structural and leaf trait variables (blue) for *k* = 2, 3, and 4 for Sepilok and *k* = 3 for Danum. All results are compared to the full 10-variable *k*-means clustering analysis for Sepilok (a) and Danum (b). LES traits: leaf economic spectrum traits which include leaf mass per area (LMA), foliar nitrogen (N) and foliar phosphorus (P).

requires careful selection of the number of clusters. Additionally, however, we gained valuable insights via the exploration of varying numbers of clusters as it relates to biologically meaningful categorization of forest types. Extending this method to other parts of the tropics will require similar decision-making, which will either require user input, or the development of robust automated algorithms for selecting *k*.

Forest types capture differences in ecosystem dynamics. We further evaluated the canopy traits and structural attributes that were most critical for mapping distinct forest types, hypothesizing that mapped forest types exhibit distinct ecosystem function. Forest types revealed by the cluster analyses were distributed along the leaf economic spectrum, where the leaf economic

spectrum characterizes a tradeoff in plant growth strategies³⁶. LMA, which can covary strongly with leaf N and P, is a key indicator of plant growth strategies along the spectrum³⁷. At the slow-return end of the leaf economics spectrum, plants in nutrient-poor conditions with low leaf nutrient concentrations invest in leaf structure and defense, expressed as high LMA, strategizing longer-lived, tougher leaves with slower decomposition rates. This strategy comes at the cost of slower growth. At the quick-return end of the spectrum, plants in nutrient-rich environments with higher leaf nutrient concentrations invest less in structure and defense, enabling faster growth and more rapid leaf turnover, i.e., shorter leaf lifespans. This quick-return growth strategy supports higher photosynthetic rates and more rapid carbon gain³⁶.

In this study, the principal components and clustering results yielded forest types that are indicative of community level differences associated with leaf economic spectrum differences. The nutrient rich sites (Danum1 and Danum2, Supplementary Fig. 8) show high canopy N and P and low LMA compared to the nutrient poor and acidic sites (Sandstone and *Kerangas*), which contributes to lower leaf photosynthetic capacity (V_{cmax}) and growth (Fig. 4b). Foliar N:P also increased with site fertility, confirming that tropical forests are primarily limited by phosphorus, and not nitrogen^{38,39}, with large implications for carbon sequestration in these forests. Orthogonal differences in canopy structure and architecture between Danum forest types and Sepilok Sandstone and Alluvial forests could be indicative of ecosystem scale differences in the sensitivity of these forests to endogenous disturbance processes⁴⁰.

The significant differences in aboveground carbon stocks and growth and mortality rates between forest types further suggests strong differences in ecosystem dynamics. In general, growth rates varied inversely to aboveground carbon, and higher aboveground carbon corresponded to lower mortality rates. As an example, the Sepilok sandstone forests, which are largely comprised of slow-growing dipterocarp species^{29,33}, had the highest median aboveground carbon (236 Mg C ha⁻¹), with higher canopy P and N, and lower LMA. The taller canopy and low canopy leaf nutrient concentrations are consistent with the low growth and mortality rates found in the sandstone forest, indicating a slow-growth strategy yielding larger trees and higher aboveground carbon stocks. In contrast, alluvial forests exhibit high turnover with mortality and growth rates higher relative to Sandstone forests corresponding to lower aboveground carbon on average. *Kerangas* forests exhibited low aboveground carbon despite an intermediate plot-level growth rate, and mortality rates that were significantly lower than the Danum or alluvial forest types. *Kerangas* forests, which were characterized by the highest LMA, lowest foliar P and N (Fig. 2a), and the lowest plot-level aboveground carbon density (186 Mg C ha⁻¹; Fig. 4a), are known to have higher stem densities, lower canopy heights, and long-lived leaves^{5,32,41}, suggesting well-developed strategies for nutrient retention⁴². Interestingly, despite significantly different aboveground carbon and demography, the *kerangas* and sandstone forests did not differ in LAI or canopy architecture (P:H); although maximum height, Cover_{20} , and H_{peak} LAI were significantly higher in the sandstone forest, highlighting the need to account for differences beyond LAI when scaling processes from leaves to ecosystems.

In addition, when three forest types were distinguished at Sepilok, the alluvial inventory plot had significantly higher aboveground carbon than the remote sensing-derived alluvial forest extent (Fig. 4a, $p < 0.001$). It was only when the mudstone and alluvial forests were differentiated when $k=4$ that the inventory plot and clustered alluvial forest areas exhibited similar aboveground carbon distributions, with significantly lower carbon in the mudstone forest. Although Sepilok mudstone and alluvial forests are often characterized as a single forest type^{5,43}, independent research first identified mudstone hills as unique based on differences in soil cation exchange capacity, pH, and nutrient concentrations that translated into intermediate plant growth rates in mudstone forests⁴⁴. More recently, higher clay fractions and higher exchangeable Mg, Ca, and K were found at varying soil depths in Sepilok mudstone forests compared to alluvial forests, although alluvial forests exhibited higher foliar N, P, K, and Mg concentrations compared to mudstone forests³⁰. Our remote sensing findings independently support the uniqueness of mudstone forests based on both leaf traits and structural attributes (Figs. 2 and 3). The lower aboveground carbon in the mudstone forest may be due to lower leaf nutrient concentrations

and higher soil acidity, as well as differences in hydrology associated with seedling and sapling responses to flooding that influence the species assembly^{45,46}. Because the mudstone forests in Sepilok are also closer to anthropogenic forest edges than alluvial forests, edge effects—which have been shown to significantly influence large tree mortality and lower aboveground carbon—may also be a factor^{47–49}.

At Danum, our results indicate that the region is comprised of one to three forest types that differ in LMA, foliar N and P, canopy height, and vertical structure (Figs. 1 and 2; Supplementary Figs. 7–8). Our finding that two of these forest types (Danum 1 and 2) were found within the 50 ha Smithsonian ForestGEO inventory plot interestingly aligns with recent, independent research. Differences in species composition and soil characteristics have been identified between the northeast corner and the remainder of the 50 ha plot³⁰. A recent study also identified the northeast corner (Danum 1) has having lower species richness, diversity, stem density, and basal area compared to the rest of the plot (Danum 2), linked to less acidic soils with a higher cation exchange capacity and higher Ca, Mg, and Ni content³¹.

Implications for modeling tropical forest biomes. We did not find significant variation in total ecosystem LAI across forest types in this study. In contrast, vertical variation in structure was more strongly linked to differences between functionally distinct forest types. LAI is considered one of the most important eco-physiological attributes of vegetation, and is widely used in terrestrial ecosystem and biosphere models to upscale estimates of leaf-level processes to ecosystems and to model land atmosphere interactions^{26,27}. LAI varies significantly among the world's biomes⁵⁰. Within tropical forests, previous studies have shown that variation is correlated with maximum water deficit, minimum temperature, and forest protection status⁵¹. However, as shown here, LAI variation does not vary significantly across the different lowland forest types (alluvial, sandstone, mudstone, and *kerangas*) found at Sepilok and Danum. Average canopy LAI (estimated from the airborne LiDAR data using the method described in ref. 52) was similar across forest types, ranging from 5 to 6. A recent study argued that total LAI may not be directly relevant for many processes in ecosystems (e.g., productivity) beyond a value of three⁵³.

However, our finding of significant variation in vertical LAI profiles, despite no substantial variation in average ecosystem LAI, provides important evidence that vertical foliar distributions may be more important than the absolute amount of leaf area for characterizing differences across ecosystems, underscoring the importance of evaluating additional LiDAR-derived metrics and leaf traits. In particular, the vertical distribution of leaf area is important for many canopy processes since the total amount of leaf surface area and its vertical organization can vary independently^{54,55}. Although terrestrial biosphere models differ in their representation of vertical forest strata, there has been a growing effort to incorporate vertical variation more directly in many models⁵⁶. Several recent model developments are at the cutting edge of representing vertical variation, which implement vertical gradients of irradiance, water content, and leaf temperature in ways that better enable models to capture differences in function within and between forest ecosystems^{57–59}.

In conclusion, we explore the ability to map forest types at the spatial resolution of forthcoming hyperspectral satellite sensors and evaluate the ability of those forest types to capture differences in three aspects of ecosystem dynamics: aboveground biomass stocks, growth rates, and mortality rates. It was beyond the scope of this study to conduct ground validation of the entire extent of the mapped forest types. However, an important next step for

further research entails a more detailed analysis of differences in forest composition, structure, and ecosystem dynamics at the larger landscape scale, beyond the inventory plots evaluated in this study. Establishing 1 ha plots and repeatedly censusing them across the extent of each forest type mapped would yield more robust accuracy assessments of the forest type maps reported here and will be critical for disentangling the mechanisms and processes underpinning differences in structure and function. Despite this need for further in situ analyses, this study provides the first step toward reliably characterizing differences in forest types over large areas, where forest inventory plots are not readily available. This type of mapping alone offers invaluable insights into differences across vast areas of tropical forest that are otherwise often characterized as a single biome in ecosystem models. The ability to capture this variation within the global critical tropical forest biome sets a new bar for terrestrial biosphere modeling. Results from this type of analysis can be used to parameterize and benchmark earth system models, further constraining high uncertainty in the future dynamics of these ecosystems.

Since the main axes of variation in canopy properties correspond to quantities measurable from spaceborne LiDAR and imaging spectroscopy, our approach offers a framework for large-scale mapping of functionally distinct forest types that can be employed across highly diverse tropical forest ecosystems at regional and global scales. Canopy leaf phosphorus (P) and leaf mass per unit area (LMA) were critical for distinguishing between forest types and will thus be essential to accurately map from spaceborne sensors for ecological applications. Maximum canopy height, and the fraction of canopy cover taller than 20 m, were important for distinguishing forest types, although variation in structure alone was insufficient to capture differences. These types of analyses at pan-tropical scales will be invaluable for improving understanding of ecosystem variation across a biome that is both incredibly threatened by and critical to mitigating global climate change. Our findings also underscore synergies between ground-based and remote-sensing ecological analyses, whereby landscape-scale remote surveys can efficiently pinpoint locations that can be targeted as high priority for discovery-oriented fieldwork and ground-based measurements.

Methods

Study landscapes. The study landscapes are in Sabah, Malaysian Borneo, encompassing forests in Danum Valley with the tallest trees in the tropics⁶⁰, and nutrient-poor *kerangas* forests with stunted canopies and unique floristic composition⁶¹. The first landscape is Sepilok, a 4500 ha reserve of lowland mixed dipterocarp forests spanning varying topography and soil nutrients^{5,32,41,44}. The second landscape is Danum, a 44,000 ha conservation area with predominantly lowland, intact tropical rain forest. In this study, we focus on the 50 ha ForestGEO inventory plot located in the eastern part of Danum.

Both landscapes exhibit differences in structure, function, and composition that correspond to underlying soil and geologic substrate^{5,33,41,43,44}. Sepilok is characterized by three forest types: alluvial forests on fertile ultisols along alluvial flats and gentle slopes; sandstone forests on well-drained, nutrient-poor ultisols along steep ridges; and *kerangas* forests that dominate acidic, extremely nutrient-poor podosols along lower dip slopes of cuesta landforms^{33,62}. Total phosphorus, nitrate, and base cations are significantly higher in alluvial soils than in the sandstone and more acidic *kerangas* forest soils, influencing forest type differences in species composition, leaf traits, and stand structure^{29,32}. An earlier field study also identified mudstone hills within the alluvial forests as being further distinguishable in terms of soil chemistry and plant growth⁴⁴, although mudstone and alluvial areas in Sepilok are typically characterized as a single forest type^{5,43}.

Airborne remote sensing data. To measure forest structure and foliar traits, we used co-aligned LiDAR and imaging spectroscopy data collected by the Global Airborne Observatory in April 2016, which are described in detail in the Supplementary Methods and in ref. ²². We examined ten forest structure variables and canopy foliar characteristics that are strongly linked to ecosystem function and have demonstrated measurability with high accuracy using airborne remote-sensing techniques (Supplementary Tables 1 and 2, Supplementary Figs. 1 and 2).

Variation in canopy structure was characterized using five metrics: 99th percentile of total canopy height (Max H, m), LAI (LAI, $m^2 m^{-2}$), the peak height of LAI ($H_{peak LAI}$, m), a measure of canopy architecture indicating the vertical distribution of plant foliage (P) relative to the total canopy height (P:H ratio), and the fraction of canopy cover taller than 20 m height above the ground (Cover₂₀, %). Variation in canopy leaf traits were analyzed based on differences in leaf mass per area (LMA, $g DM m^{-2}$), foliar nitrogen (N, %) and phosphorus (P, %) concentrations, and foliar N:P ratios. To assess differences in maximum photosynthetic capacity, V_{cmax} was estimated from remotely sensed maps of leaf N and P using the equation in Table 3, model 1 from²⁵. Estimated V_{cmax} was not validated with in situ ecophysiology measurements and is thus simply meant to provide an additional axis of functional variation in this study. To examine the feasibility of conducting these analyses at coarser resolutions, we resampled data and ran analyses at resolutions ranging from 16 m^2 to 40,000 m^2 . LiDAR and imaging spectroscopy data and processing are described in Supplementary Methods.

Characterizing functionally distinct forests. We mapped forest types across Sepilok and Danum. At Danum, we restricted our analysis to the 50 ha ForestGEO plot location and a 1 km buffer around the plot. To characterize functional and structural diversity across all pixels, we (1) conducted a PCA to reduce dimensionality of all ten canopy leaf traits and structural attributes (hereafter canopy properties), and (2) ran a *k*-means cluster analysis²⁸ on the first two principal components to categorize pixels into functionally distinct forest types. PCA and *k*-means cluster analysis data processing is described in Supplementary Methods.

The primary metric for identifying the appropriate number of clusters (*k*) was the gap statistic (Gap_{*k*}), which defines the number of clusters based on the first local and global maxima³⁵. We also evaluated output for $k = k_s + 1$ and for $k = k_s - 1$, where k_s represents the number of clusters selected using Gap_{*k*}. Two secondary cluster metrics were also considered: (1) the elbow approach using the within group sum of squares (W_k), and (2) the BSS divided by the TSS. A higher value of BSS/TSS indicates improved fit of the cluster analysis to the data⁶³. Because BSS/TSS increases monotonically as *k* increases, we evaluated the *k* at which BSS/TSS increases flattened, in addition to Gap_{*k*} and the W_k elbow approach³⁵.

We visually evaluated cluster results against inventory plot data from forest ecosystems that have been studied extensively in the field and exhibit clear differences in structure and function. Significant differences in canopy properties between clusters were calculated based on one-way ANOVAs using the *aov* and *TukeyHSD* functions from the *stats* base package in R⁶⁴. To explore the minimum number of canopy properties required to capture differences in forest types, we evaluated cluster results using only LiDAR variables (structural attributes), only imaging spectroscopy variables (leaf traits), and reduced combinations of canopy properties. To evaluate these reduced models, we calculated overall accuracy as the proportion of pixels mapped the same as the full 10-variable model.

Inventory plot data. To evaluate cluster analysis performance, we compared our forest type maps to inventory plot data at Danum and Sepilok. Our plot dataset consisted of nine existing 4 ha forest inventory plots distributed across alluvial ($n = 3$), sandstone ($n = 3$), and *kerangas* ($n = 3$) forests at Sepilok, and one 50 ha plot at Danum. Data from the nine 4 ha Sepilok plots and the Danum 50 ha plot were from the ForestPlots.net online repository⁶⁵ and the ForestGEO online repository⁶⁶, respectively. The datasets include stem diameter measurements and taxonomic identification to species level for every tree ≥ 1 cm and ≥ 5 cm in diameter in the ForestGEO and ForestPlots.net plots, respectively. Census years from each plot were as follows: alluvial—2001, 2009, 2014; sandstone—2001/03, 2008/09, 2013/14; *kerangas*—2001, 2008/10, 2014/15; Danum—2011/15, 2019. The Global Airborne Observatory campaign in Sabah was conducted in 2016.

Observed differences in ecosystem properties. In lieu of direct measurements of ecosystem function at the study locations (e.g., net primary productivity), we quantified differences in three related ecosystem properties: aboveground carbon, growth, and mortality. We compared stand-level growth and mortality rates calculated from forest inventory data and remotely sensed estimates of aboveground carbon density (ACD, $Mg C ha^{-1}$)—including stem, branch, and leaf biomass—at plot locations within the inventory plots, and across all mapped pixels within each forest type to examine differences in aboveground carbon beyond the plots. ACD at 30 m resolution was estimated from the Global Airborne Observatory top-of-canopy height (TCH) and Cover₂₀ data following⁶⁷, described in ref. ⁶⁸. The method involves estimating ACD from a network of 0.25 to 1 ha field plots using the BIOMASS workflow described in conjunction with the pan-tropical biomass allometry^{69,70}. Equations from⁷¹, modified by⁶⁸, were used to estimate ACD from the TCH data, modified based on⁶⁷ to incorporate Cover₂₀ as a proxy for stand-level basal area. Annual relative DBH growth rates and annual mortality rates were calculated from plot data (stems ≥ 10 cm) following⁷². When calculating growth rates, we excluded trees with broken or resprouted stems and stems that grew >7.5 cm yr^{-1} or shrunk $>25\%$ of their initial DBH following⁷². Negative growth rates $<25\%$ of initial DBH were converted to zero.

Data availability

The data associated with this paper are published on Zenodo via the Global Airborne Observatory account and can be found via the searchable DOIs cited below. *Trait Maps*: Global Airborne Observatory foliar trait maps for Sepilok Forest Reserve and the Danum Valley ForestGEO 50-ha plot with a 1 km buffer in Sabah, Malaysia derived from imaging spectroscopy data collected 31 March to 30 April 2016: Foliar N, Foliar P, Leaf Mass per Area (LMA) rasters. <https://doi.org/10.5281/zenodo.7051897>; https://zenodo.org/record/7051897#.YxZ_m3bMJpZ. *LiDAR*: Global Airborne Observatory LiDAR data for Sepilok Forest Reserve and the Danum Valley ForestGEO 50 ha plot with a 1 km buffer in Sabah, Malaysia collected 31 March to 30 April 2016: Top-of-canopy height (TCH), P.H, Leaf Area Density (LAD), rasters. <https://doi.org/10.5281/zenodo.7051897>; https://zenodo.org/record/7051897#.YxZ_m3bMJpZ.

Code availability

Code to organize, resample, and merge data for application of PCA and k-means clustering. Also includes code to estimate V_{cmax} , and calculate Leaf Area Index (LAI) from Leaf Area Density (LAD), Peak height of LAI (PeakLAI), and $Cover_{20}$. <https://doi.org/10.5281/zenodo.7052347>; <https://zenodo.org/record/7052347#.YxbQnHbMJpY>.

Received: 28 October 2021; Accepted: 23 September 2022;

Published online: 20 October 2022

References

- Corlett, R. T. Plant diversity in a changing world: Status, trends, and conservation needs. *Plant Divers.* **38**, 10–16 (2016).
- Hubau, W. et al. Asynchronous carbon sink saturation in African and Amazonian tropical forests. *Nature* **579**, 80–87 (2020).
- Liu, J. et al. Contrasting carbon cycle responses of the tropical continents to the 2015–2016 El Niño. *Science*. **358**, eaam5690 (2017).
- Givnish, T. J. On the causes of gradients in tropical tree diversity. *J. Ecol.* **87**, 193–210 (1999).
- Jucker, T. et al. Topography shapes the structure, composition and function of tropical forest landscapes. *Ecol. Lett.* **21**, 989–1000 (2018).
- Townsend, A. R., Asner, G. P. & Cleveland, C. C. The biogeochemical heterogeneity of tropical forests. *Trends Ecol. Evol.* **23**, 424–431 (2008).
- Hulshof, C. M. & Spasojevic, M. J. The edaphic control of plant diversity. *Glob. Ecol. Biogeogr.* **29**, 1634–1650 (2020).
- Chazdon, R. L. Tropical forest recovery: legacies of human impact and natural disturbances. *Perspect. Plant Ecol. Evol. Syst.* **6**, 51–71 (2003).
- Brando, P. M. et al. Droughts, Wildfires, and Forest Carbon Cycling: A Pantropical Synthesis. *Annu. Rev. Earth Planet. Sci.* **47**, 555–581 (2019).
- Draper, F. C. et al. Imaging spectroscopy predicts variable distance decay across contrasting Amazonian tree communities. *J. Ecol.* **107**, 696–710 (2019).
- Bongalov, B. et al. Reconciling the contribution of environmental and stochastic structuring of tropical forest diversity through the lens of imaging spectroscopy. *Ecol. Lett.* **22**, 1608–1619 (2019).
- Asner, G. P. et al. Airborne laser-guided imaging spectroscopy to map forest trait diversity and guide conservation. *Science* **355**, 385–389 (2017).
- Antonarakis, A. S., Munger, J. W. & Moorcroft, P. R. Imaging spectroscopy and lidar-derived estimates of canopy composition and structure to improve predictions of forest carbon fluxes and ecosystem dynamics. *Geophys. Res. Lett.* **41**, 2535–2542 (2014).
- Féret, J. B. & Asner, G. P. Mapping tropical forest canopy diversity using high-fidelity imaging spectroscopy. *Ecol. Appl.* **24**, 1289–1296 (2014).
- Chadwick, K. D. & Asner, G. P. Geomorphic transience moderates topographic controls on tropical canopy foliar traits. *Ecol. Lett.* **23**, 1276–1286 (2020).
- ESA, E. S. A. PRISMA (Hyperspectral Precursor and Application Mission). *eoPortal Directory* (2021). <https://directory.eoportal.org/web/eoportal/satellite-missions/p/prisma-hyperspectral>. (Accessed: 19th June 2021).
- GAC, G. A. C. & TBE, T. B. E. DESIS: DLR Earth Sensing Imaging Spectrometer. *Teledyne* (2021). <https://tbe.com/geospatial/desis>. (Accessed: 19th June 2021).
- Dubayah, R. et al. The Global Ecosystem Dynamics Investigation: High-resolution laser ranging of the Earth's forests and topography. *Sci. Remote Sens.* **1**, 100002 (2020).
- Cawse-Nicholson, K. et al. NASA's surface biology and geology designated observable: a perspective on surface imaging algorithms. *Remote Sens. Environ.* **257**, 112349 (2021).
- ESA, E. S. A. CHIME (Copernicus Hyperspectral Imaging Mission for the Environment). *eoPortal Directory* (2021). <https://directory.eoportal.org/web/eoportal/satellite-missions/c-missions/chime-copernicus>. (Accessed: 19th June 2021).
- Martin, R. E. et al. An approach for foliar trait retrieval from airborne imaging spectroscopy of tropical forests. *Remote Sens.* **10**, 199 (2018).
- Asner, G. P. et al. Carnegie Airborne Observatory-2: Increasing science data dimensionality via high-fidelity multi-sensor fusion. *Remote Sens. Environ.* **124**, 454–465 (2012).
- Wright, S. J. et al. Functional traits and the growth-mortality trade-off in tropical trees. *Ecology* **91**, 3664–3674 (2010).
- Bruehlheide, H. et al. Global trait-environment relationships of plant communities. *Nat. Ecol. Evol.* **2**, 1906–1917 (2018).
- Walker, A. P. et al. The relationship of leaf photosynthetic traits - V_{cmax} and J_{max} - to leaf nitrogen, leaf phosphorus, and specific leaf area: A meta-analysis and modeling study. *Ecol. Evol.* **4**, 3218–3235 (2014).
- Jarvis, P. G. & McNaughton, K. G. Stomatal Control of Transpiration: Scaling Up from Leaf to Region. *Adv. Ecol. Res.* **15**, 1–49 (1986).
- Bonan, G. B., Pollard, D. & Thompson, S. L. Influence of subgrid-scale heterogeneity in leaf area index, stomatal resistance, and soil moisture on grid-scale land-atmosphere interactions. *J. Clim.* **6**, 1882–1897 (1993).
- Hartigan, J. A. & Wong, M. A. Algorithm AS 136: A K-Means Clustering Algorithm. *J. R. Stat. Soc. Ser. C (Applied Stat.)* **28**, 100–108 (1979).
- Dent, D. H. & Burslem, D. F. R. P. Performance trade-offs driven by morphological plasticity contribute to habitat specialization of bornean tree species. *Biotropica* **41**, 424–434 (2009).
- Bartholomew, D. et al. Differential nutrient limitation controls leaf physiology, supporting niche partitioning in tropical dipterocarp forests. *Funct. Ecol.* **36**, 2084–2103 (2021).
- Cardon Pocovi, J.M. Drivers of species richness, tree community composition and diversity in a lowland dipterocarp forest in Sabah, Malaysia. *MSc thesis, Univ. Aberdeen, UK* 1–46 (2019).
- Dent, D. H., Bagchi, R., Robinson, D., Majalap-Lee, N. & Burslem, D. F. R. P. Nutrient fluxes via litterfall and leaf litter decomposition vary across a gradient of soil nutrient supply in a lowland tropical rain forest. *Plant Soil* **288**, 197–215 (2006).
- Dent, D. H. & Burslem, D. F. R. P. Leaf traits of dipterocarp species with contrasting distributions across a gradient of nutrient and light availability. *Plant Ecol. Divers.* **9**, 521–533 (2016).
- Baldeck, C. A. & Asner, G. P. Estimating Vegetation Beta Diversity from Airborne Imaging Spectroscopy and Unsupervised Clustering. *Remote Sens.* **5**, 2057–2071 (2013).
- Tibshirani, R., Walther, G. & Hastie, T. Estimating the number of clusters in a data set via the gap statistic. *Stat. Methodol.* **63**, 411–423 (2001).
- Wright, I. J. et al. The worldwide leaf economics spectrum. *Nature* **428**, 821–827 (2004).
- Osnas, J. L. D. et al. Divergent drivers of leaf trait variation within species, among species, and among functional groups. *Proc. Natl. Acad. Sci. USA* **115**, 5480–5485 (2018).
- Fleischer, K. et al. Amazon forest response to CO₂ fertilization dependent on plant phosphorus acquisition. *Nat. Geosci.* **12**, 736–741 (2019).
- Quesada, C. A. et al. Basin-wide variations in Amazon forest structure and function are mediated by both soils and climate. *Biogeosciences* **9**, 2203–2246 (2012).
- Russo, S. E. et al. The interspecific growth-mortality trade-off is not a general framework for tropical forest community structure. *Nat. Ecol. Evol.* **5**, 174–183 (2021).
- Fox, J. E. D. *A handbook to Kabili-Sepilok Forest Reserve*, Sabah Forest Record No. 9., Sandakan, Sabah Forestry Department, 1–102 (1973).
- Turner, I. M. A Quantitative Analysis of Leaf Form in Woody Plants from the World's Major Broadleaved Forest Types. *J. Biogeogr.* **21**, 413 (1994).
- Coomes, D. A. et al. Area-based vs tree-centric approaches to mapping forest carbon in Southeast Asian forests from airborne laser scanning data. *Remote Sens. Environ.* **194**, 77–88 (2017).
- Nilus, R. Effect of edaphic variation on forest structure, dynamics, diversity and regeneration in a lowland tropical rainforest in Borneo. *PhD thesis, (Univ. Aberdeen, UK)*, 2004).
- Born, J. et al. Differing Life History Characteristics Support Coexistence of Tree Soil Generalist and Specialist Species in Tropical Rain Forests. *Biotropica* **46**, 58–68 (2014).
- Born, J. et al. Differential Responses of Dipterocarp Seedlings to Soil Moisture and Microtopography. *Biotropica* **47**, 49–58 (2015).
- Ordway, E. M. & Asner, G. P. Carbon declines along tropical forest edges correspond to heterogeneous effects on canopy structure and function. *Proc. Natl. Acad. Sci. USA* **117**, 7863–7870 (2020).
- Qie, L. et al. Long-term carbon sink in Borneo's forests halted by drought and vulnerable to edge effects. *Nat. Commun.* **8**, 1–11 (2017).
- Laurance, W. F., Delamónica, P., Laurance, S. G., Vasconcelos, H. L. & Lovejoy, T. E. Rainforest fragmentation kills big trees. *Nature* **404**, 836 (2000).
- Fang, H., Baret, F., Plummer, S. & Schaepman-Strub, G. An Overview of Global Leaf Area Index (LAI): Methods, Products, Validation, and Applications. *Rev. Geophys.* **57**, 739–799 (2019).

51. Pfeifer, M. et al. Tropical forest canopies and their relationships with climate and disturbance: results from a global dataset of consistent field-based measurements. *For. Ecosyst.* **5**, 1–14 (2018).
52. Detto, M., Asner, G. P., Muller-Landau, H. C. & Sonnentag, O. Spatial variability in tropical forest leaf area density from multireturn lidar and modeling. *J. Geophys. Res. Biogeosci.* **120**, 294–309 (2015).
53. Parker, G.G. Tamm review: Leaf Area Index (LAI) is both a determinant and a consequence of important processes in vegetation canopies. *For. Ecol. Manage.* **477**, 1–15 (2020).
54. Wu, J., Liu, Y. & Jelinski, D. E. Effects of leaf area profiles and canopy stratification on simulated energy fluxes: The problem of vertical spatial scale. *Ecol. Modell.* **134**, 283–297 (2000).
55. Shugart, H. H., Saatchi, S. & Hall, F. G. Importance of structure and its measurement in quantifying function of forest ecosystems. *J. Geophys. Res. Biogeosci.* **115**, 1–16 (2010).
56. Fisher, R. A. & Koven, C.D. Perspectives on the Future of Land Surface Models and the Challenges of Representing Complex Terrestrial Systems. *J. Adv. Model. Earth Syst.* **12**, e2018MS001453 (2020).
57. Chen, X., Massman, W. J. & Su, Z. A Column Canopy-Air Turbulent Diffusion Method for Different Canopy Structures. *J. Geophys. Res. Atmos.* **124**, 488–506 (2019).
58. Bonan, G. B. et al. Modeling canopy-induced turbulence in the Earth system: a unified parameterization of turbulent exchange within plant canopies and the roughness sublayer (CLM-ml v0). *Geosci. Model Dev.* **11**, 1467–1496 (2018).
59. Longo, M. et al. The biophysics, ecology, and biogeochemistry of functionally diverse, vertically and horizontally heterogeneous ecosystems: The Ecosystem Demography model, version 2.2-Part 2: Model evaluation for tropical South America. *Geosci. Model Dev.* **12**, 4347–4374 (2019).
60. Shenkin, A. et al. The World's Tallest Tropical Tree in Three Dimensions. *Front. For. Glob. Chang.* **2**, 1–5 (2019).
61. Newbery, D. M. Floristic variation within kerangas (heath) forest: re-evaluation of data from Sarawak and Brunei. *Vegetatio* **96**, 43–86 (1991).
62. DeWalt, S. J., Ickes, K., Nilus, R., Harms, K. E. & Burslem, D. F. R. P. Liana habitat associations and community structure in a Bornean lowland tropical forest. *Plant Ecol.* **186**, 203–216 (2006).
63. Milligan, G. W. & Cooper, M. C. An examination of procedures for determining the number of clusters in a data set. *Psychometrika* **50**, 159–179 (1985).
64. R Core Team. R: A language and environment for statistical computing. R Foundation for Statistical Computing <https://www.r-project.org/> (2022).
65. ForestPlots.net, et al. Taking the pulse of Earth's tropical forests using networks of highly distributed plots. *Biol. Conserv.* **260**, 1–27 (2021).
66. ForestGEO. ForestGEO Data Portal. *Global Earth Observatory Network* (2021). <http://ctfs.si.edu/datarequest/>. (Accessed: 13th July 2020).
67. Jucker, T. et al. Estimating aboveground carbon density and its uncertainty in Borneo's structurally complex tropical forests using airborne laser scanning. *Biogeosciences* **15**, 3811–3830 (2018).
68. Asner, G. P. et al. Mapped aboveground carbon stocks to advance forest conservation and recovery in Malaysian Borneo. *Biol. Conserv.* **217**, 289–310 (2018).
69. Réjou-Méchain, M., Tanguy, A., Piponiot, C., Chave, J. & Hérault, B. BIOMASS: an R package for estimating above-ground biomass and its uncertainty in tropical forests. *Methods Ecol. Evol.* **8**, 1163–1167 (2017).
70. Chave, J. et al. Improved allometric models to estimate the aboveground biomass of tropical trees. *Glob. Chang. Biol.* **20**, 3177–3190 (2014).
71. Asner, G. P. et al. A universal airborne LiDAR approach for tropical forest carbon mapping. *Oecologia* **168**, 1147–1160 (2012).
72. Condit, R. et al. The importance of demographic niches to tree diversity. *Science* **313**, 98–101 (2006).

Acknowledgements

E.O. was supported by the Harvard University Center for the Environment Postdoctoral Fellowship program (PM, mentor). The airborne science was completed with funding

from the United Nations Development Programme and donations to GA from the Avatar Alliance Foundation, Margaret A. Cargill Foundation, David and Lucile Packard Foundation, Gordon and Betty Moore Foundation, Grantham Foundation for the Protection of the Environment, W. M. Keck Foundation, John D. and Catherine T. MacArthur Foundation, Andrew Mellon Foundation, Mary Anne Nyburg Baker and G. Leonard Baker Jr., and William R. Hearst III, and Arizona State University. Plots at Sepilok were funded by the British Ecological Society, with the re-census in 2013 carried out by RN and LQ funded by an ERC Advanced Grant to OLP (291585, T-FORCES). The Danum plot is a core project of the Southeast Asia Rain Forest Research Partnership (SEARRP). We thank SEARRP partners, especially Yayasan Sabah for their support, and HSBC Malaysia and the University of Zurich for funding. We are grateful to the research assistants who are conducting the census, in particular the team leader Alex Karolus, and to Mike Bernados and Bill McDonald for species identifications. We thank Stuart Davies and Shameema Esufali for advice and training. This contribution is an output of ForestPlots.net approved research project no. 46, entitled, Unraveling the role of prior disturbance histories in heterogeneous tropical forest responses to climate change.

Author contributions

E.O. and P.M. designed the study. D.B., S.L., R.N., M.O., O.P., and L.Q. collected and provided the inventory plot data. G.A. and R.E.M. led the collection of remote sensing data and foliar trait data. R.E.M. and N.V. processed the remote sensing data and foliar chemical data. E.O. analyzed the output data, performed the statistical modeling work, and wrote the first draft of the paper.

Competing interests

The authors declare no competing interests.

Additional information

Supplementary information The online version contains supplementary material available at <https://doi.org/10.1038/s43247-022-00564-w>.

Correspondence and requests for materials should be addressed to Elsa M. Ordway.

Peer review information *Communications Earth & Environment* thanks Thomas Janssen and the other, anonymous, reviewer(s) for their contribution to the peer review of this work. Primary Handling Editors: Erika Buscardo and Clare Davis. Peer reviewer reports are available.

Reprints and permission information is available at <http://www.nature.com/reprints>

Publisher's note Springer Nature remains neutral with regard to jurisdictional claims in published maps and institutional affiliations.



Open Access This article is licensed under a Creative Commons Attribution 4.0 International License, which permits use, sharing, adaptation, distribution and reproduction in any medium or format, as long as you give appropriate credit to the original author(s) and the source, provide a link to the Creative Commons license, and indicate if changes were made. The images or other third party material in this article are included in the article's Creative Commons license, unless indicated otherwise in a credit line to the material. If material is not included in the article's Creative Commons license and your intended use is not permitted by statutory regulation or exceeds the permitted use, you will need to obtain permission directly from the copyright holder. To view a copy of this license, visit <http://creativecommons.org/licenses/by/4.0/>.

© The Author(s) 2022